Predictions of the cycle-to-cycle aerodynamic loads on a yawed wind turbine blade under stalled conditions using a 3D empirical stochastic model

MOUTAZ ELGAMMI[1] and TONIO SANT[1]
[1]Department of Mechanical Engineering, University of Malta, Msida MSD 2080, Malta

E-mail: *moutaz.elgammi.13@um.edu.mt*

Abstract. This paper investigates a new approach to model the stochastic variations in the aerodynamic loads on yawed wind turbines experienced at high angles of attack. The method applies the one-dimensional Langevin equation in conjunction with known mean and standard deviation values for the lift and drag data. The method is validated using the experimental data from the NREL Phase VI rotor in which the mean and standard deviation values for the lift and drag are derived through the combined use of blade pressure measurements and a free-wake vortex model. Given that direct blade pressure measurements are used, 3D flow effects arising from the co-existence of dynamic stall and stall delay are taken into account. The model is an important step towards verification of several assumptions characterized as the estimated standard deviation, Gaussian white noise of the data and the estimated drift and diffusion coefficients of the Langevin equation. The results using the proposed assumptions lead to a good agreement with measurements over a wide range of operating conditions. This provides motivation to implement a general fully independent theoretical stochastic model within a rotor aerodynamics model, such as the free-wake vortex or blade-element momentum code, whereby the mean lift and drag coefficients can be estimated using 2D aerofoil data with correction models for 3D dynamic stall and stall delay phenomena, while the corresponding standard derivations are estimated through CFD.

Nomenclature

C_D	drag coefficient
C_L	lift coefficient
C_N	normal force coefficient
C_T	tangential force coefficient
$D^{(1)}$	drift coefficient
$D^{(2)}$	diffusion coefficient
f_s	frequency (Hz)
M	conditional moment
N	sample size
r	local radial position (m)
R	tip radius (m)
t	time (sec)
T_{bin}	length of the time period at each bin
V_n	normal flow velocity (m/s)
V_t	tangential flow velocity (m/s)
U_∞	free stream wind speed (m/s)
X	C_L, C_D, C_N, C_T sample data vector
α	angle of attack **(**rad**)**
μ	mean
μ_{CD}	mean of drag force coefficient
μ_{CL}	mean of lift force coefficient
σ	standard deviation
τ	total time period (sec)
τ_0	time increment (sec)
Φ	yaw angle (deg)
Ψ	blade azimuth angle (deg)
Γ_B	bound circulation (m^2/s)
Γ_G	Gaussian white noise (Langevin force**)**

1. Introduction

Wind turbine design procedures still rely considerably on the use of models that are unable to simulate the real unsteady aerodynamic behaviour experienced at high angles of attack. Wind tunnel measurements conducted under controlled conditions have evidently shown that wind turbines in yaw experience a significant cycle-to-cycle variability in aerodynamic loads at high angles of attack [1]. Such behaviour was observed even under simple flow conditions involving a steady and uniform wind flow. The unsteady aerodynamic loads can sometimes also be observed under attached flow conditions characterized as amplitude and phase variations compared to quasi-steady flow conditions [2].

Various models have been developed to simulate the unsteady aerodynamic loads associated with dynamic stall. Examples include the Beddeos and Leishman model [2], the Onera model [3], Øye model [4] and the Risø *fgh* model [5]. However, these models still depend on 2D aerofoil wind tunnel data and various semi-empirical models that usually cater for 3D aerodynamic phenomena such as stall delay. These models are not able to simulate the stochastic cycle-to-cycle variations in the aerodynamic loads experienced by the rotor under yawed conditions.

Several studies have been performed to evaluate the stochastic behaviour of the unsteady aerodynamic loads based on measured data from 2D wind tunnels. Bertagnolio *at et*. [6] established a stochastic approach to model the unsteady effects on a blade exhibiting a static stall originating from the self-induced turbulent wake of an aerofoil. The input data to the model can be measured data or determined by a CFD code for aerofoil sections at constant angles of attack. The model was also applied for wind turbines giving interesting insight on the characteristics of stall. Luhur *et al. [*7] recently developed a stochastic model based on the Langevin stochastic differential equation [8] to model the dynamic lift and drag force coefficients on an aerofoil under turbulent wind inflow conditions. The work aimed at replacing the 2D typical lookup tables of the static lift and drags force coefficients by the dynamic response of the lift and drag forces. Luhur *et al*. [9] further extended the latter work for wind turbine applications. The stochastic model was integrated with the blade element momentum (BEM) model in order to predict the dynamic forces on a rotating blade. Although the model showed clear insight on the time history of the aerodynamic loads, applications of the model for a full scale wind turbine were not provided to demonstrate efficiency of the model. Stochastic models have been also used to simulate turbulent atmospheric flows and their effects on the power performance of wind turbines as shown in work of Wächter *et al*. [10] and Gottschall [11].

To the authors' knowledge, stochastic modelling of the aerodynamic loads to capture the unsteady effects of stalled conditions in yawed rotors is very limited. This work is a first attempt to develop a new approach to simulate such a stochastic behaviour. The analysis is based on the NREL Phase VI rotor that was tested in the NASA Ames wind tunnel [1]. The main scope is to use experimental data for aerodynamic loading for the yawed rotor to verify some assumptions important for developing a general fully independent stochastic model. The mean and standard deviation values for the lift and drag coefficients derived from such data are used as input in the stochastic model to predict the cycle-to-cycle aerodynamic based on the principles of Gaussian white noise and the one-dimensional stochastic Langevin equation [8]. Through the verification of the various assumptions in the present paper, it will be possible to evaluate the potential for developing a general fully independent stochastic model in wind turbine aerodynamic design codes such as those based on the Blade-Element-Momentum (BEM) or free wake vortex (FWV) methods where the mean values of lift and drag coefficients are predicted via 2D aerofoil data with correction models for 3D effects arising from dynamic stall and stall delay phenomena while the corresponding standard deviation values are determined using Computational Fluid Dynamics (CFD).

2. NASA Ames UAE Wind Tunnel Data

For validation of the proposed 3D empirical stochastic model, the two bladed NREL wind turbine rotor Phase VI is used [1]. This model is a 10.1*m* diameter HAWT tested in the NASA Ames

24.38*m*×36.57*m* wind tunnel. The blade sections have the geometric profile of the S809 aerofoil. The case study presented here is for the upwind baseline configuration with a 3^0-tip pitch angle, a 0^0-cone angle and a constant rotational speed of 71.6 rpm. Analysis in this study was restricted to a free wind speed of 15*m/s* and a yaw angle of 30^0. This paper only considered the experimental data collected with the 'H' configurations (see ref. [1]).

3. Methodology Overview

This section presents the theoretical principles required to build the proposed 3D empirical stochastic model. Overviews on these principles are presented as follows:

3.1 Data Sampling

The normal and tangential force coefficient data were binned per one-degree azimuth angle. Therefore, each individual bin includes a total of 30 data points, each corresponds to an individual rotor rotation. The analysis in the remaining sections of this paper was conducted at these samples/bins. Figure 1 illustrates some samples/bins for these data at U_∞=15 *m/s* at *r/R*=0.30 at $\Phi=30^0$.

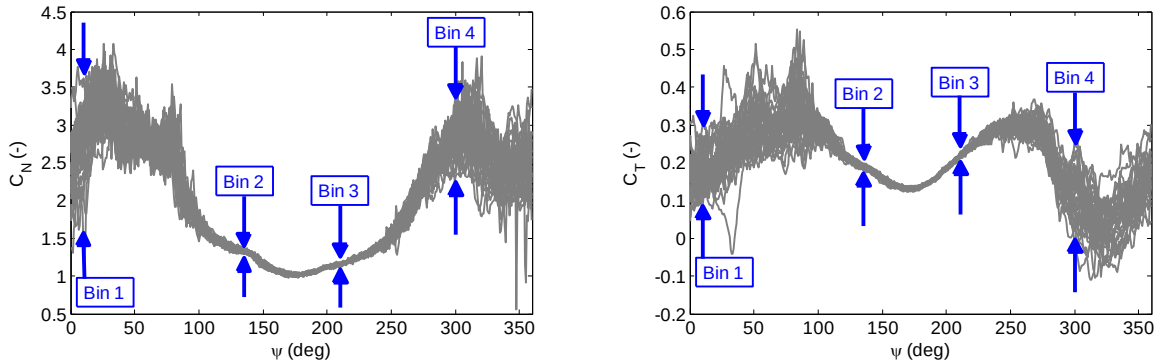

(a) Normal force coefficient (b) tangential force coefficient

Figure 1: Variation of normal and tangential force coefficients with blade azimuth angle at U_∞=15 *m/s* at *r/R*=0.30 at $\Phi=30^0$. Arrows indicate a selection of data bins for statistical analysis.

3.2 Normality Test for the Cycle-to-Cycle Aerodynamic Loads

This subsection presents normality tests carried out using the Shapiro-Wilk p-value (*p-value>0.05*) [12] to identify the type of distribution of the aerodynamic loads along all radial locations and blade azimuth angles over 30 rotor rotations. Shapiro-Wilk's test analyzes the hypothesis of normality based on a random sample. It is defined as the ratio of the best estimator of the variance to the usual corrected sum of squares estimator of the variance. Further details can be found in [12]. Figure 2 shows results from the Shapiro-Wilk p-value test for the normal and tangential force coefficients at U_∞*=15m/s* and $\Phi=30^0$. From this test, the percentage numbers of data points having non-normal distribution are 10.74% for C_N and 13.51% for C_T. Hence, it could be reliably assumed that all data are normally distributed for engineering analysis.

3.3 Testing characteristics of White Noise of the Cycle-to-Cycle Aerodynamic Loads

The autocorrelation function of a continuous random signal can be defined as a condition in which the samples are uncorrelated and identically distributed with variance equal to σ^2. A white noise process is, on the other hand, a random process with a flat power spectral density (*PSD*). Power spectral density function illustrates how much power is included in each of the spectral component and describes the distribution of the power of a signal with respect to its frequencies [13]. According to Wiener-Khintchine Theorem [14], the Fourier Transform of auto-correlation function of a random process is used to calculate the power spectral density function of the random process. The measured C_N and C_T data was binned per one degree azimuth angle (see Figure 1, Subsection 3.1). Figure 3 shows the auto-correlation function and the power spectral density of C_N and C_T white noise (with zero

mean values) determined at wind speed 15*m/s* at yaw angle 30^0 at r/R=0.30 at bin 1 given in Figure 1. In Figure 3, the auto-correlation function for C_N and C_T indicates that the C_N and C_T white noise data are zero everywhere except at time lag zero (variance equal to σ^2 at zero time lag) meaning that samples/variables are statistically uncorrelated with respect to each other. This condition satisfies the defined white noise process with variance (σ^2) equal to variance or power of the corresponding C_N and C_T white noise data at zero time lags. On the other hand, the power spectral density (*PSD*) of the C_N and C_T white noise data across 30 rotations gives almost fixed power in all the frequency domain (-∞ to +∞). The same observation was also found for all other azimuth angle bins for the different radial locations.

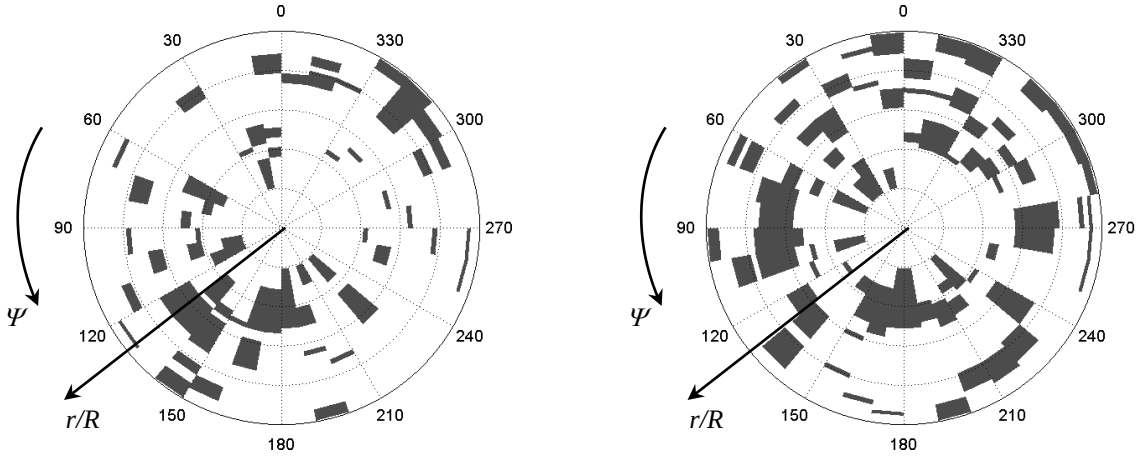

(a) C_N *(b) C_T*

Figure 2: Normally and non-normally distributed C_N and C_T data at U_∞=15*m/s* and Φ=30^0. Dark colour indicates the non-normally distributed data (*p-value* ≤ 0.05), while the white colour indicates the normally distributed data (*p-value* > 0.05).

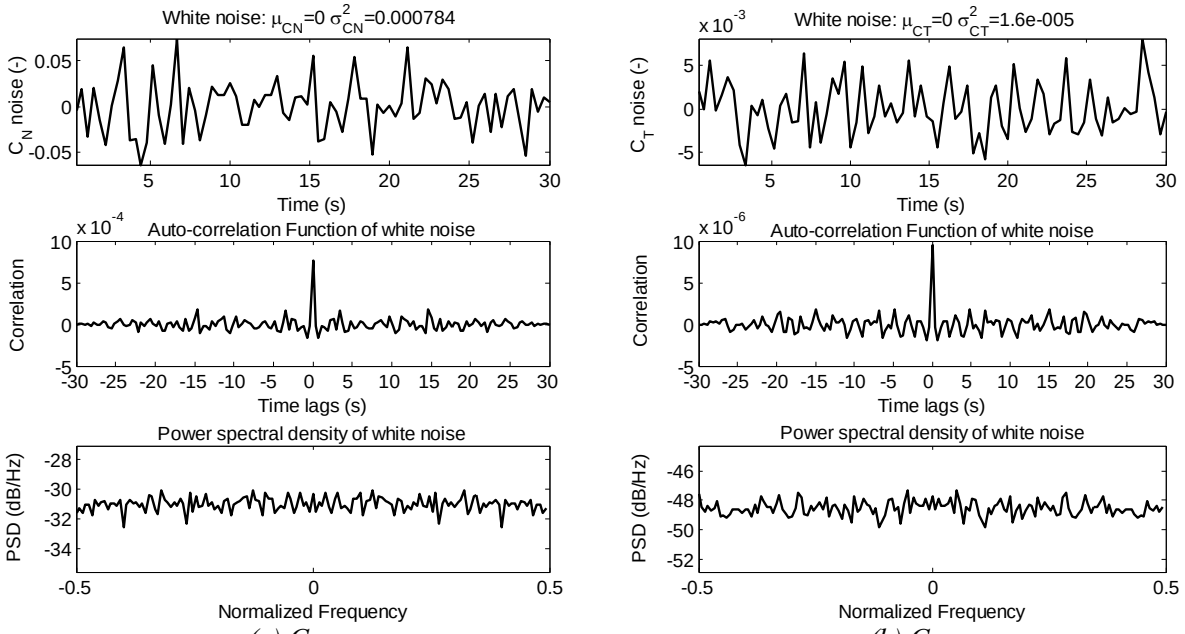

(a) C_N *(b) C_T*

Figure 3: Power spectral density and auto-correlation function of C_N and C_T white noise at U_∞=15*m/s* and Φ=30^0 at r/R=0.30 at Ψ=0.

3.4 Gaussian White Noise (GWN) Process

In order to model a Gaussian white noise process, the standard Gaussian random variable is a commonly used model for a random/stochastic process as given by:

$$X = \mu + \sigma.Normal(0,1) \tag{1}$$

where *Normal*(*0, 1*) is a random process with zero mean and standard deviation equal to unity, X denotes the lift or drag time series. μ is the mean of lift or drag force which can be determined directly from measurements or from 2D aerofoil data and correction models for 3D dynamic stall/stall delay implemented in a rotor aerodynamics code (such as FWV/BEM codes). σ is the standard deviation of the lift or drag force which can be either measured data or predicted by a CFD code capable of simulating the unsteady aerodynamic loads. To apply equation 1, the optimal sample size should be evaluated as follows:

Optimal Number of Samples

The optimal number of samples is of great importance for Monte Carlo simulation (MCS) as this stochastic technique is mainly based on the use of random numbers to analyze problems of interest. The number of samples cannot be randomly selected as this may lead to significant errors in the results. In this study, the number of samples is selected according to convergence of standard deviation of the investigated parameters; the lift and drag force coefficients using different sets of random numbers as input values to equation 1. Thus, the number of samples was gradually increased from 0 up 150,000 and the corresponding converged standard deviations of the lift and drag force coefficients were determined as shown in Figure 4. From Figure 4, it is obvious that 100,000 samples are sufficient for successful Monte Carlo simulation (MCS) as it is guaranteed that the standard deviation of such samples is not affected by the sample size, while those below 5000 samples are significantly impacted by the sample size. Hence, samples with 100,000 random variables were mainly used for the current verifications and analysis in this study.

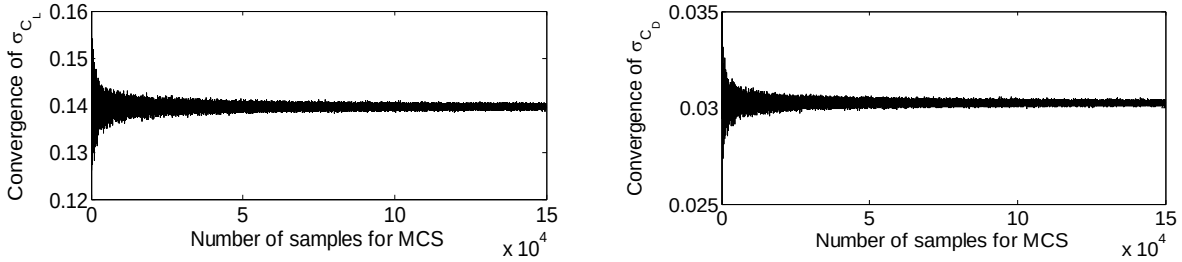

Figure 4: Illustration for convergence of standard deviation of lift force coefficient to select the optimal number of samples for MCS at U_∞=15*m/s* and Φ=30^0 at *r/R*=0.30 at Ψ=0^0.

3.5 One-Dimensional Stochastic Langevin Equation

The prediction of the aerodynamic loads when moving from one cycle/rotor rotation to another at each time step is achieved by applying a first-order stochastic differential equation based on drift and diffusion coefficients (the Langevin equation [8]) as given by:

$$\frac{dX(t)}{dt} = D^{(1)}(X) + \sqrt{D^{(2)}(X)}\,\Gamma_G(t) \tag{2}$$

where X denotes the lift or drag force coefficient, and $\Gamma_G(t)$ is Gaussian white noise named as Langevin force [8] with mean ($\langle \Gamma_G(t) \rangle$=0) and variance ($\langle \Gamma^2_G(t) \rangle$=2), where $\langle \cdot \rangle$ represents the average over time. $D^{(1)}(X)$ is the drift term presenting the deterministic part of the Langevin equation and it estimates the mean change or mean time derivative of the aerodynamic loads. $D^{(2)}(X)$ is the diffusion term presenting the stochastic part which is characterized as the fluctuations in the

aerodynamic loads since it quantifies the random noisy fluctuations together with $\Gamma_G(t)$. The drift and diffusion coefficients can be reconstructed directly from measured data (Siegert *et. al* [15], Gottschall and Peinke [16]) with the use of:

$$D^n(X,\psi) = \frac{1}{n!}\,\tau \lim_{\tau \to 0} \frac{1}{\tau} M^{(n)}(X,\tau) \tag{3}$$

where $M^{(n)}$ is the first (n=1) and second (n=2) conditional moment respectively as expressed by

$$M^{(n)}(X,\tau) := \langle [X(t+\tau) - X(t)]^n \rangle \Big|_{X(t)=X;\Psi} \tag{4}$$

The drift and diffusion coefficients are determined by dividing the lift and drag force coefficient time series in each sample by the number of bins. Equations 3 and 4 are then applied for $X(t) = X$ in each bin. The drift coefficient $D^{(1)}(X)$ is determined using n=1, while the diffusion coefficient $D^{(2)}(X)$ is calculated using n=2. Since the Langevin force term, $\Gamma_G(t)$, in Equation 2 involves a Gaussian white noise process (a random process), it cannot be assumed that the estimated new stochastic signal, representing the aerodynamic loads at each time step, is accurate. This means that several stochastic signals will be differ from one another as determined by the term $\Gamma_G(t)$. In order to have a reliable estimate of the new stochastic signal of the aerodynamic loads at each time step, Monte Carlo simulation (MCS) is performed based on averaged converged standard deviation of different sets of estimated stochastic signals as shown in Figure 5. It is apparent that Monte Carlo simulation (MCS) requires at least 2000 stochastic signals to successfully provide accurate estimation of the aerodynamic loads at each time step.

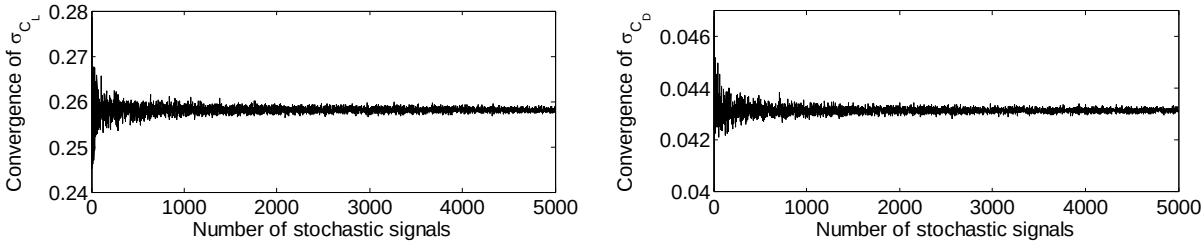

Figure 5: Illustration for convergence of averaged standard deviation of lift and drag force coefficient across different numbers of stochastic signals for MCS at U_∞=10m/s and Φ=45^0 at r/R=0.30 at Ψ=0^0.

4. NREL Rotor Lift and Drag Data for Validation of 3D Empirical Stochastic Model

The proposed stochastic model requires input of both the mean and standard deviation of the lift and drag coefficient data for the different rotor blade radial locations and azimuth angles. Such data should take into consideration the 3D effects associated with both dynamic stall and stall delay phenomena normally experienced by yawed rotors operating with high angles of attack at the blades. To validate the proposed model, unsteady lift and drag coefficient data for the NREL rotor were used. These were derived directly using the iterative procedure developed by Sant *et al.* [18] which applies a free-wake vortex model to determine the angle of attack α from the blade normal and tangential load coefficient data obtained from the blade pressure measurements. In the present study, the free-wake vortex model *WInDS* developed by Sebastian [17] was adopted, allowing the estimation of the time history of the time-varying angle of attack α for 30 consecutive rotor rotations, hence accounting for cycle-to-cycle variability. A detailed description of this iterative approach may be found in [19]. The time history for α was then used with the measured data for the normal and tangential loads to extract the corresponding aerodynamic lift and drag coefficients over the 30 rotor evaluations. Finally, the latter values were used to obtain the mean (μ_{CL} and μ_{CD}) and standard deviation (σ_{CL} and σ_{CD}) values to be used as input to the stochastic model. It should be noted that given that direct measured load data were used, then 3D flow effects resulting from stall delay and dynamic stall phenomena, as well as those associated with the blade flow at the tip, are already taken into account. The standard deviations were extracted from the 3D experimental data under various wind speeds and yaw angles as illustrated in

Figure 7. These were eventually used as 2D lookup tables in the developed 3D empirical stochastic model when modelling the cycle-to-cycle variations of the aerodynamic loads.

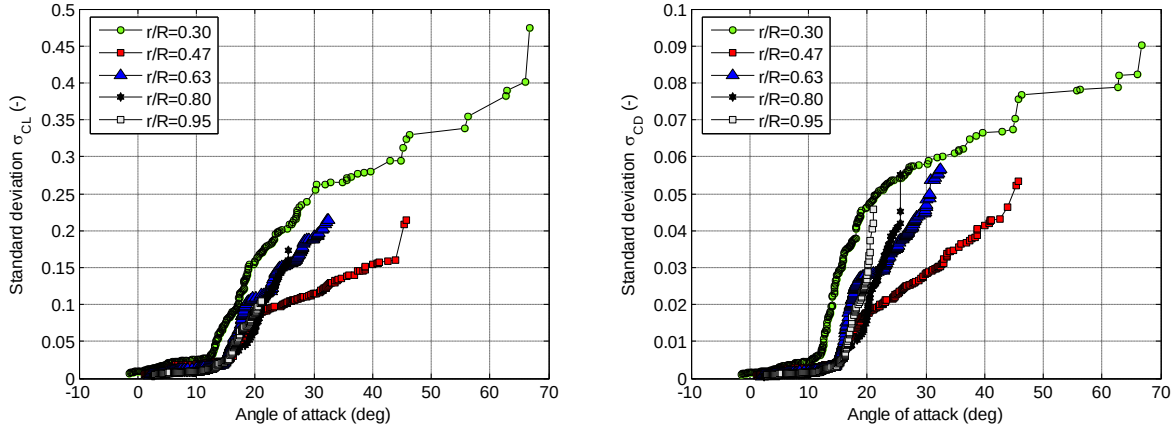

Figure 6: Standard deviations of the lift and drag force coefficients derived from the NREL rotor phase VI at several radial locations, wind speeds and yaw angles.

5. Numerical Algorithm of the 3D Empirical Stochastic Model

This section describes the numerical algorithm of the stochastic model when implemented in the free-wake vortex model *WInDS* [17]. The aerodynamic quantities obtained from the NREL rotor blade pressure measurements described in Section 4 above (α, μ_{CL} and μ_{CD}, σ_{CL} and σ_{CD}) were used as input to predict the cycle-to-cycle aerodynamic loads on a rotating blade of the NREL rotor. The following procedure was applied over successive 36 azimuth angle steps (blade rotational increments of 10^0):

1. For each new time step, 100,000 random variables (samples) are generated for each individual bin following Gaussian white noise (see Equation 1 and Subsection 3.4). These are added to the mean experimental aerodynamic lift and drag force coefficients, $\mu_{CL}|_{\Psi=0}$ and $\mu_{CD}|_{\Psi=0}$ determined from the first stage (Section 4) as given by:

$$C_L|_{initial} = \mu_{CL}|_{\Psi=0} + \sigma_{CL}|_{\Psi=0}.Normal(0,1) \quad (5)$$

$$C_D|_{initial} = \mu_{CD}|_{\Psi=0} + \sigma_{CD}|_{\Psi=0}.Normal(0,1) \quad (6)$$

   where σ_{CL} and σ_{CD} are the standard deviation of the lift and drag force coefficients. These are computed from the 2D lookup tables generated using the data plotted in Figure 6.

2. The drift coefficients, $D^{(1)}(C_L|_{initial}, \Psi)$ and $D^{(1)}(C_D|_{initial}, \Psi)$, and the diffusion coefficients, $D^{(2)}(C_L|_{initial}, \Psi)$ and $D^{(2)}(C_D|_{initial}, \Psi)$, are determined from the 100,000 samples generated in Step 1 of the second stage and Equations 3 and 4. The value of drift can be estimated by fitting a linear function, while the diffusion can be predicted by a second-order polynomial with least square regression scheme applied for each case. Figure 7 illustrates sample results for the estimated $D^{(1)}(C_L|_{initial}, \Psi)$ and $D^{(2)}(C_L|_{initial}, \Psi)$ at $\Psi=300^0$ / (bin 4 in Figure 1) at U_∞= 15*m/s* and $\Phi=30^0$ at r/R=0.30.

3. The Langevin process (Equation 2) is then applied to determine the lift and drag force coefficients at ($\Psi=0^0$) or (t=0) over 30 successive rotor rotations as given in the discrete form by:

$$C_L|_{\Psi=0} = \mu_{CL}|_{\Psi=0} + \tau_0\, D^{(1)}(C_L|_{initial}, \Psi) + \sqrt{\tau_0\, D^{(2)}(C_L|_{initial}, \Psi)}\; Normal(0,\sqrt{2}) \quad (7)$$

$$C_D|_{\Psi=0} = \mu_{CD}|_{\Psi=0} + \tau_0\, D^{(1)}(C_D|_{initial}, \Psi) + \sqrt{\tau_0\, D^{(2)}(C_D|_{initial}, \Psi)}\; Normal(0,\sqrt{2}) \quad (8)$$

   where $Normal(0,\sqrt{2})$ is Gaussian white noise with mean 0 and variance 2. The time increment τ_0 is equal to the inverse sampling rate. This may be replaced by the sampling

frequency of the actual values. Equations 7 and 8 are solved by Monte Carlo Simulation using 2000 stochastic random signals as explained in Subsection 3.5 and shown in Figure 8.

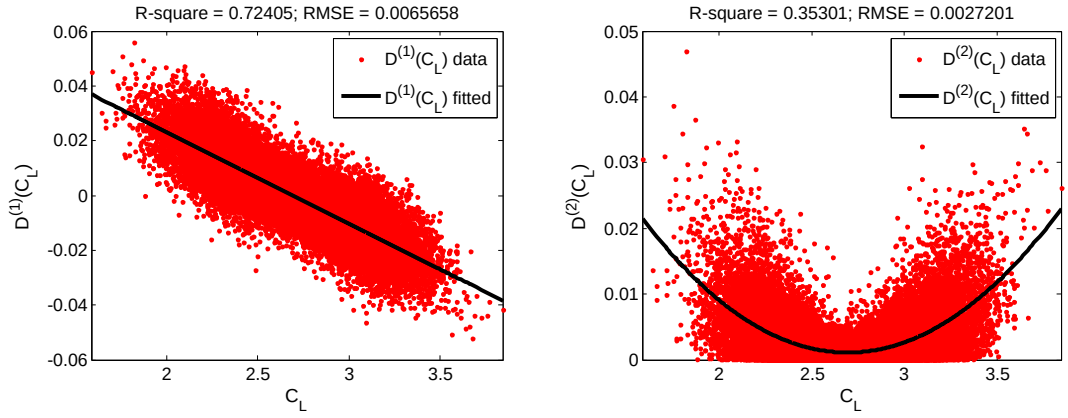

(a) $D^{(1)}(C_L, \Psi)$ *(b) $D^{(2)}(C_L, \Psi)$*

Figure 7: Estimated drift and diffusion coefficients of C_L and C_D at Ψ=300^0/ (bin 4 in Figure 1) at U_∞= 15*m/s* and Φ=30^0 at 0.30*R*.

4. Because the aerodynamic loads deviate around the mean C_L and C_D values at each blade azimuth angle across 30 rotor rotations (see Figure 8), the model was extended to present the aerodynamic load oscillations for the current time step over 30 rotor rotations as follows:

$$C_L\big|_{model} = C_L\big|_{\Psi=0} + \frac{1}{2}\sigma_{CL}\cos(2\pi\tau_0 f_s) \tag{9}$$

$$C_D\big|_{model} = C_D\big|_{\Psi=0} + \frac{1}{2}\sigma_{CD}\cos(2\pi\tau_0 f_s) \tag{10}$$

where f_s is the frequency of the wave ($f_s = 1/T_{bin}$), where T_{bin} is the length of the time period at each azimuth angle or bin presented in Figure 1. In Figure 8, the grey color represents the generated 2000 stochastic signals which have been already verified in Figure 5. The solid black markers denote the estimated averaged solution over the 2000 stochastic signals determined by Equations 9 and 10. Each individual marker represents the predicted value at each individual rotor rotation at each new time step and each individual bin.

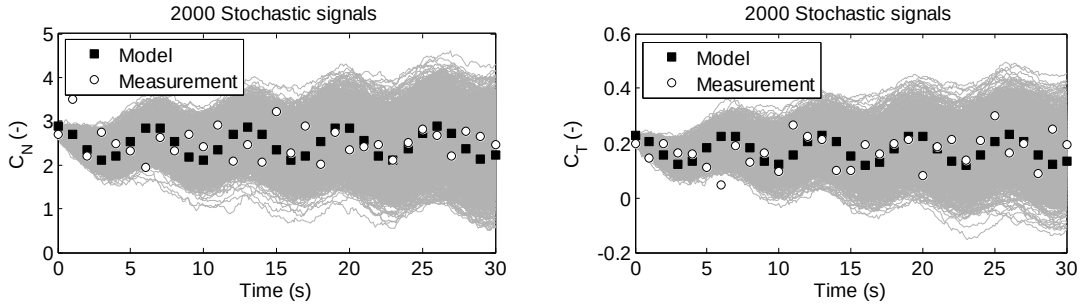

Figure 8: Unsteady normal and tangential force coefficients predicted by the extended model (Equation 9 and 10) at U_∞= 15*m/s*, Φ=30^0, *r/R*=0.30 at bin 1 in Figure 1.

5. A necessary step to ensure that the predictions of the aerodynamic loads at each time step are reliable is to check for any predicted values outside the 99% confidence interval. It is crucial to make sure that 99% of the predicted aerodynamic loads always contain the true value. This is achieved to obtain the final unsteady cycle-to-cycle aerodynamic lift and drag force coefficients as follows:

$$C_L\big|_{final} = C_L\big|_{model} \pm \frac{2.58 \cdot \sigma_L}{\sqrt{N}} \tag{11}$$

$$C_D\big|_{final} = C_D\big|_{model} \pm \frac{2.58 \cdot \sigma_D}{\sqrt{N}} \tag{12}$$

where N is the sample size (N=100,000).

6. The bound circulations, Γ_B, are computed using the Kutta-Joukowksi theorem using Equation 13 and the cycle-to-cycle lift force coefficients $C_L|_{final}$.

$$\Gamma_B = \frac{1}{2}.C_L\big|_{final} V_{rel}.c \tag{13}$$

7. The free wake downstream for the current time step is generated to determine the 3D unsteady induced velocities on the lifting line and all wake nodes via Biot-Savart law over 30 rotor rotations. The angle of attack is then determined by:

$$\alpha = \tan^{-1}(V_n / V_t) \tag{14}$$

8. The cycle-to-cycle normal and tangential force coefficients are then determined by Equations 15 and 16.

$$C_N = C_L\big|_{final} \cos(\alpha) + C_D\big|_{final} \sin(\alpha) \tag{15}$$

$$C_T = C_L\big|_{final} \sin(\alpha) - C_D\big|_{final} \cos(\alpha) \tag{16}$$

Steps 1-8 are repeated for all time steps and radial locations over a whole rotor rotation (36 time steps).

6. Results

Sample results from the 3D empirical stochastic model are presented in Figure 9 for three individual rotor rotations, 10th, 20th and 30th, at wind speed 15*m/s* and a yaw angle 30^0 at the 30% span location. Comparisons over 30 rotor rotations are also achieved at U_∞= 15*m/s* at Φ=30^0 at 0.30*R* and 0.8*R* as illustrated in Figure 10. It is observed that there is in general very good agreement between the measurements and the predictions. Some slight under/over prediction can be observed in Figure 9 due to assumptions and estimations made in this study. It was previously assumed that all data follow a normal distribution for each blade radial and azimuth position, but in fact some small regions do not really follow Gaussian distributions (Figure 2). It is also expected that the determined drift and diffusion coefficients suffer from errors created by the strong measurement noise as well as the curve fitting procedure (Figure 7). Despite these, it is shown that the stochastic model is successfully capable of reproducing the cycle-to-cycle variability in the load coefficients experienced at blade azimuth positions having a large angle of attack. Indeed, the averaged loads are already affected by the dynamic stall phenomenon, while the unstable/random process of the dynamic stall vortex shedding causes the variations around the mean values from cycle (revolution) to another. Hence, the model is able to capture the effects of the 3D dynamic stall vortex shedding at high angles of attack relatively well. On the other hand, the strategy of the binning process presented in Figure 1 would simplify the complexity of the process used in the developed 3D stochastic model when moving from a bin to another (i.e. when progressing with time). Such binning process would typically reduce the correlation between the samples/bins given that the averaged values of C_N and C_T at each new bin are either measurements or determined by a dynamic stall and stall delay models integrated with a rotor aerodynamics code (as for example FWV or BEM codes). The results shown in Figures 9 and 10 indicate that the used binning process is still valid to provide an acceptable level of accuracy.

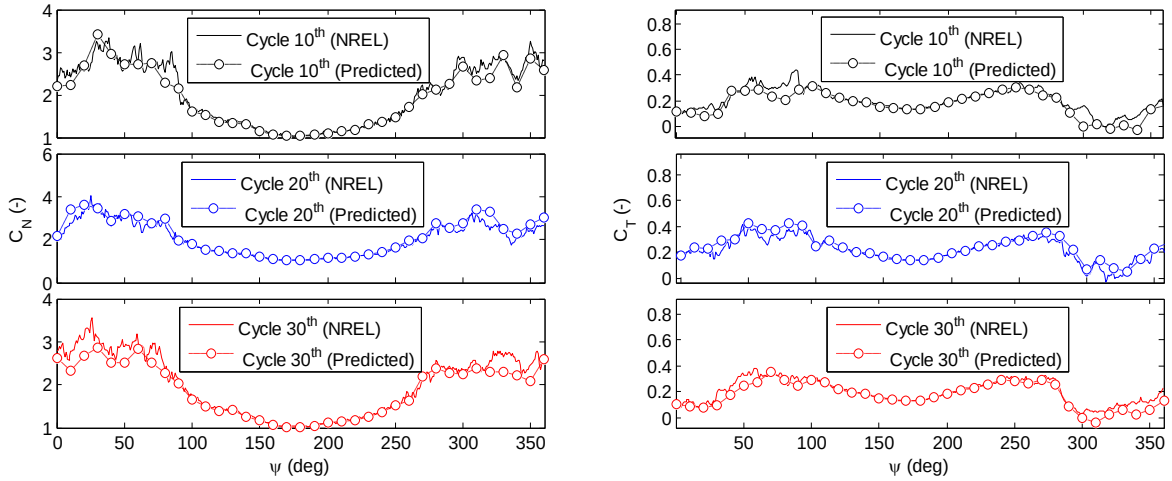

Figure 9: A comparison between measured and predicted normal and tangential force coefficients at U_∞= 15*m/s* at Φ=30^0 at 0.3*R*. These are results of 10th, 20th and 30th individual rotor rotations.

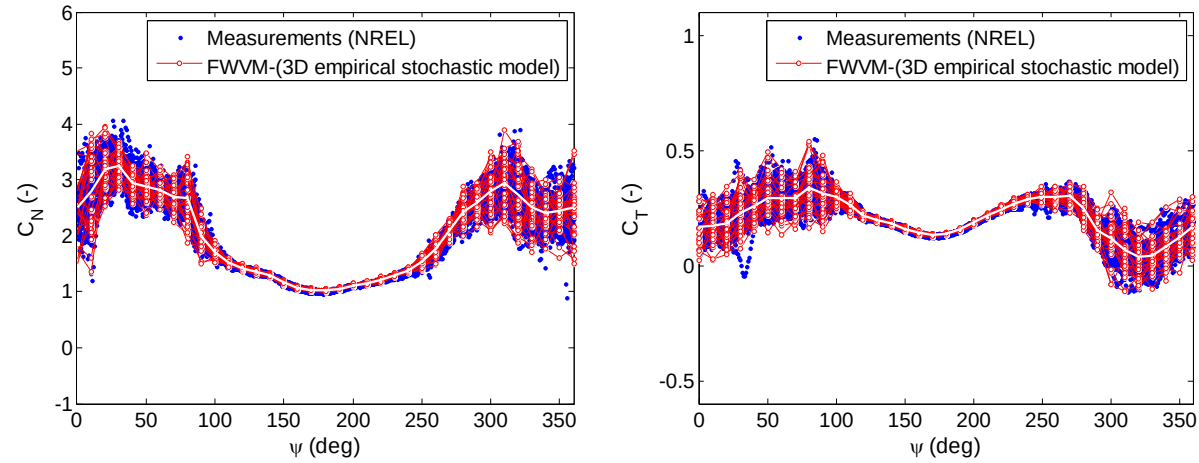

(a) 0.30R

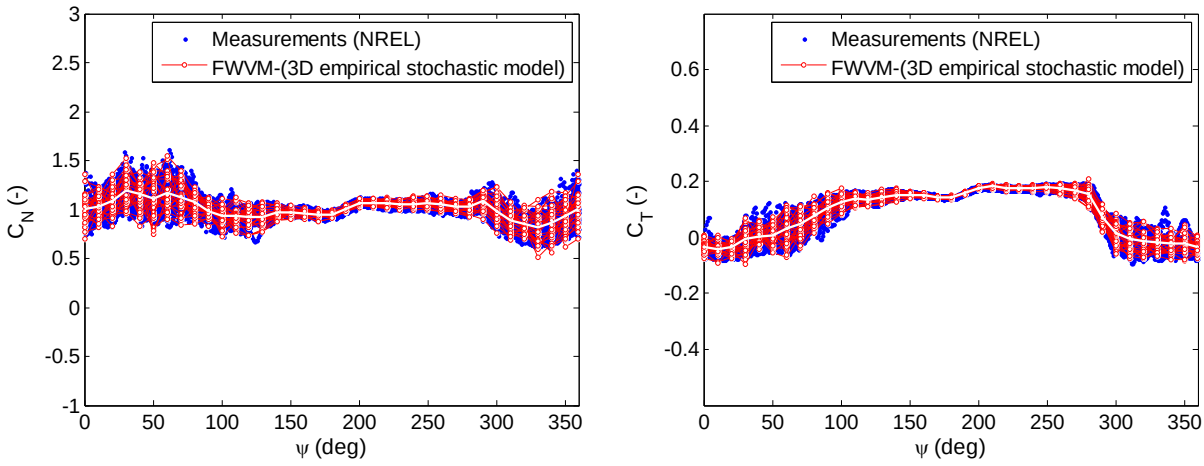

(b) 0.80R

Figure 10: A comparison between measured and predicted normal and tangential force coefficients at U_∞= 15*m/s* at Φ=30^0 at 0.3*R* and 0.8*R*. Results are shown for 30 rotor rotations.

7. Conclusions

A 3D empirical stochastic model has been developed and applied to predict the cycle-to-cycle aerodynamic loads on the blades of the NREL Phase VI rotor under yawed conditions. The results presented here show that the assumptions and approximations (the standard deviation, the normally distributed data, the estimated drift and diffusion coefficients and the white Gaussian noise principles) used within the 3D empirical stochastic model should provide sufficient accuracy to develop a fully theoretical stochastic model for wind turbine design applications. The model presented in this paper was based on the input of the mean and standard deviation values of aerodynamic loads from the NREL wind tunnel measurements. Further work is intended to apply the same technique with the use of dynamic stall and stall delay models integrated in a FWV or BEM model to independently predict the mean values of the aerodynamic loads instead of using measurement data, while the standard deviation data can be obtained from a CFD code. Further work will also test the developed model with different wind turbine rotors for which blade aerodynamic load distribution measurements are available over multiple rotations.

References

[1] Hand M M, Simms D A, Fingersh L J, Jager D W, Cortell J R, Schreck S and Larwood S M 2001 Unsteady Aerodynamics Experiments Phase VI: Wind Tunnel Test Configurations and Available Data Campaigns; Technical Report NREL/TP-500-29955; *National Renewable Energy Laboratory*: Golden, CO, USA.

[2] Leishman J G 2002 Challenges in Modelling the Unsteady Aerodynamics of Wind Turbines. *Wind Energy*, **5**: 85–132. doi: 10.1002/we.62.

[3] Peters D A 1985 Toward a Unified Lift Model for Use in Rotor Blade Stability Analysis. *Journal of American Helicopter Society*; **30**(3): 32-42.

[4] Øye S 1991 Dynamic stall simulated as time lag of separation, Technical report, Department of Fluid Mechanics, *Technical University of Denmark*, Denmark.

[5] Rasmussen F 1995 Engineering model for dynamic stall. Risø-M-854. *Risø National Laboratory*.

[6] Bertagnolio F 2010 Rasmussen F., Sørensen N.N., Johansen J., Madsen H.A, A stochastic model for the simulation of wind turbine blades in static stall, *Wind Energy*; **13**(4): 323-338. doi: 10.1002/we.342.

[7] Luhur M R, Peinke J, Schneemann J and Wächter M 2014 Stochastic modeling of lift and drag dynamics under turbulent wind inflow conditions, *Wind Energy*. doi: 10.1002/we.1699.

[8] Risken H 1996 *The Fokker–Planck Equation: Methods of Solution and Applications*, 2nd ed.; Springer: Berlin, Germany; **18**: 32-62.

[9] Luhur M R, Peinke J J, Kühn M M, Wächter M M 2015 Stochastic Model for Aerodynamic Force Dynamics on Wind Turbine Blades in Unsteady Wind Inflow. *ASME. J. Comput. Nonlinear Dynam.* **10**(4):041010-041010-10. doi:10.1115/1.4028963.

[10] Wächter M, Milan P, Mücke T and Peinke J 2011 Power performance of wind energy converters characterized as stochastic process: applications of the Langevin power curve. Wind Energy, **14**: 711–717. doi:10.1002/we.453.

[11] Gottschall J 2009 Modelling the variability of complex systems by means of Langevin processes: On the application of a dynamical approach to experimental data, PhD thesis, The Carl von Ossietzky University of Oldenburg, Germany.

[12] Shapiro S S and Wilk M B 1965 *An analysis of variance test for normality (complete samples)*. Biometrika; **52**(3-4): 591–611. doi:10.1093/biomet/52.3-4.591. JSTOR 2333709. MR 205384.

[13] Brillinger D R and John W 2002 Tukey's work on time series and spectrum analysis. *The Annals of Statistics*, **30**(6): 1595-1618.

[14] Chatfield C 1989 *The Analysis of Time Series-An Introduction*, 4st edition, Chapman and Hall, London; 94–95. ISBN 0-412- 31820-2.

[15] Siegert S, Friedrich R and Peinke J 1998 Analysis of data sets of stochastic systems. In: *Physics Letters A* 243, 275-280.
[16] Gottschall J and Peinke J 2008 On the definition and handling of different drift and diffusion estimates. *New Journal of Physics*, **10** 083034.
[17] Sebastian T 2012 The Aerodynamic and Near Wake of an Offshore Floating Horizontal Axis Wind Turbine. Ph.D. Thesis, *University of Massachusetts*, Amherst, MA, USA.
[18] Sant T, van Kuik G A M and van Bussel G J W 2008 Estimating the Angle of Attack from Blade Pressure Measurements on the NREL Phase VI Rotor using a Free-Wake Vortex Model: Yawed Conditions. *Wind Energy*; **12**(1): 1-32. doi:10.1002/we.280.
[19] Elgammi, M. and Sant, T., Combining Unsteady Blade Pressure Measurements and a Free-Wake Vortex Model to Investigate the Cycle-to-Cycle Variations in Wind Turbine Aerodynamic Blade Loads in Yaw. *Energies* 2016, ***9***(6), 460, doi:10.3390/en9060460.